
The Statistical Significance of the Inclusion of Graph Neural Networks in the Financial Time Series Forecasting Problem

Marco Gregnanin^{*1,2} Johannes De Smedt^{*2} Giorgio Gnecco^{*1} Maurizio Parton^{*3}

Abstract

Forecasting univariate time series in the financial market is a challenging endeavor. While numerous statistical and machine learning models have been introduced to address this challenge, they typically concentrate solely on analyzing temporal patterns within the time series data. In this research, we study the statistical significance of the inclusion of geometric patterns in enhancing forecasting accuracy within the context of time series analysis. We introduce the Time-Geometric model, a combination of models designed to exploit both geometric and temporal patterns. The contribution of this research lies in advancing the domain of univariate time series prediction, as demonstrated through extensive empirical evaluations. Our findings underscore that leveraging geometric patterns, captured through Graph Neural Networks, yields statistically significant improvements in forecasting accuracy.

1. Introduction

Univariate time series forecasting remains a challenging task due to inherent noise within the data, with no universally accepted method for noise removal and pattern identification (Bishop, 2016). Financial time series, in particular, pose additional challenges due to their stochastic nature (Tsay, 2005; Lamberton & Lapeyre, 2011).

Various methods, spanning statistical, financial mathematical, and deep learning models, address the forecasting problem for financial time series. Statistical models like AutoRegressive Integrated Moving Average (ARIMA) (Box et al., 2015) assume stationarity in stock prices. Financial mathematical models leverage Geometric Brownian mo-

tion (Black & Scholes, 1973) and jump processes (Tankov & Cont, 2003). Deep learning models, such as Recurrent Neural Networks (RNNs) (Goodfellow et al., 2016), Transformers (Vaswani et al., 2017), and Temporal Convolutional Networks (TCNs) (Lea et al., 2016), have shown success in exploiting temporal patterns within univariate time series (Elman, 1990; Hua et al., 2019). However, these models predominantly focus on temporal patterns, and the performance improvements demonstrated often lack an analysis of statistical significance, made according to established criteria (Demšar, 2006).

This research investigates the statistical significance of the inclusion of geometric patterns in enhancing forecasting accuracy for various types of time series models, including RNNs, Transformers, and TCNs. By representing univariate time series as graphs, we transition from Euclidean to non-Euclidean spaces, enabling the identification of complex patterns through graph structures, as indicated by the degree distribution. The ability to discern fractal, random, or periodic time series, particularly relevant in financial markets, is facilitated through the graph-based approach (Lacasa et al., 2008; Mandelbrot, 2013). Graph Neural Networks (GNNs) (Scarselli et al., 2008) prove effective in capturing geometric patterns by iteratively aggregating information from neighboring nodes in a graph (Hamilton et al., 2017). To address this, we propose a model combination named the “Time-Geometric” model, which combines baseline time series neural network models with dynamic GNNs. We leverage the visibility graph method (which is traditionally applied in complex network analysis) to derive a graph representation of a univariate time series. Our contributions include:

1. The introduction of the Time-Geometric model, which combines time series neural network models with dynamic GNNs;
2. Its extensive evaluation across 90 financial univariate time series, which reveals performance improvements when considering geometric patterns;
3. A statistical analysis of the results, based on both a pairwise and a multiple comparison approach, which highlights metric-dependent statistical differences among models.

^{*}Equal contribution ¹Laboratory for the Analysis of complex Economic Systems (AXES), IMT School for Advanced Studies Lucca, Italy ²Research Centre for Information Systems Engineering (LIRIS), KU Leuven, Belgium ³Department of Economic Studies, University of Chieti–Pescara, Italy. Correspondence to: Marco Gregnanin <marco.gregnanin@imtlucca.it>.

The paper is structured as follows: Section 2 reviews relevant GNN models for time series and statistical comparisons among different algorithms; Section 3 defines the research problem; Section 4 outlines the proposed model; Section 5 analyzes our proposed model compared to baseline models; Section 6 studies the statistical significance of the inclusion of geometric patterns, and finally, Section 7 concludes the paper.

2. Related Works

In this section, we provide a comprehensive review of relevant GNN models applied to time series and discuss pertinent research on multiple comparisons among algorithms. For an in-depth exploration of the forecasting problem for univariate time series, incorporating both statistical and deep learning models, please refer to Appendix A.

GNNs have demonstrated success across diverse domains, including traffic forecasting, network analysis, recommendation systems, and analysis of biological and chemical data (Wu et al., 2021). Noteworthy GNN models include the Spatio-Temporal Graph Convolutional Network (STGCN) (Yu et al., 2018) for traffic prediction, the Spectral Temporal GNN (StemGNN) (Cao et al., 2020) tested on real-world time series datasets (e.g., traffic forecasting, COVID-19), the Temporal Graph Convolutional Network (T-GCN) (Zhao et al., 2020) for traffic prediction, Graph Wavelet Neural Networks (GWNNs) (Xu et al., 2019) for classification tasks, and Graph Recurrent Neural Networks (GRNNs) (Ruiz et al., 2020) for earthquake epicenter, traffic, and epidemic tracking prediction. Specifically in the financial domain, models like multi-modality GNN (MAGNN) (Cheng et al., 2022) analyzed two Chinese stock exchanges, and Graph WaveNet with Self-Attention (Zhao et al., 2023) implemented the GWNN model to predict crude oil prices. Temporal and Heterogeneous GNN (THGNN) (Xiang et al., 2022) focused on predicting the United States and Chinese stock market behaviors. However, these models are primarily designed for multivariate time series, deriving graph representations from correlation matrices, attention mechanisms, or geographical features. Contrary to this, in Lazcano et al. (2023), the authors derived the graph representation of the crude oil prices using the visibility graph method to predict them.

Furthermore, in machine learning research, time-series models are often compared with various baseline models without a rigorous statistical analysis of the differences in results. Exceptions include Barrera-Animas et al. (2022) comparing machine learning models for predicting rainfall, Shih & Rajendran (2019) comparing statistical and deep learning models for blood supply. A deep statistical analysis was made in Parmezan et al. (2019) comparing different time series models over 95 datasets, and revealing no statistical differences in the results. Lastly, Demšar (2006) analyzed the statistical significance of several classifier models pro-

posed at the International Conference on Machine Learning from 1999 to 2003.

To summarize, GNN models are generally applied to multivariate time series forecasting problems without undergoing statistical tests on the obtained results. Additionally, classical univariate time series models rely solely on the autoregressive nature of the time series, neglecting geometric patterns.

3. Problem Formulation

This research aims to demonstrate the statistical significance of the inclusion of geometric patterns in enhancing the predictive capacity of baseline neural network models for univariate financial time series forecasting.

Let \mathbf{S} represent a collection of F univariate time series, each comprising realizations over T discrete time steps and denoted as $S^i = \{S_1^i, \dots, S_T^i\}$, $i \in \{1, \dots, F\}$. The initial step involves defining a mapping function, $f(\cdot)$, capable of predicting the future q values of a univariate target time series, denoted as S^* and chosen from \mathbf{S} , based on the graph-based representation G of the target time series and the collection of $F' \leq F$ univariate time series correlated with S^* . Consequently, the problem is formulated as learning the function f in such a way that

$$S_{t+1:t+q}^* = f(G_t, X_t). \quad (1)$$

Here, G_t represents the graph representation of the target time series S^* , obtained by considering the set $S_t^* = \{S_{t-m+1}^*, \dots, S_t^*\}$ of its past m observations up to time t , and X_t denotes an associated feature matrix, constructed by considering the set $S_t^i = \{S_{t-m+1}^i, \dots, S_t^i\}$, $i \in \{1, \dots, F'\}$ of the last m observations from each univariate time series S^i from \mathbf{S} that is correlated with S^* , which are represented in a tabular format. Additionally, a baseline function $g(\cdot)$ is defined as the mapping function predicting the future q values of S^* based solely on X_t :

$$S_{t+1:t+q}^* = g(X_t). \quad (2)$$

The subsequent step involves evaluating the performance of K learning algorithms, obtained from $f(\cdot)$ and $g(\cdot)$ over N different datasets. Let v_u^j represent the value assumed by an evaluation metric of the j -th algorithm, computed on the u -th dataset. The aim is to assess whether the evaluation metric differences among the algorithms, both in pairwise and multiple comparisons, are statistically significant. To achieve this, two key assumptions are considered:

Assumption 3.1 (Evaluation metrics comparison). A decrease in the value of the evaluation metric from v_u^1 to v_u^2 implies that algorithm $j = 2$ performs better than algorithm $j = 1$.

Assumption 3.2 (Reliability). The evaluation metrics v_u^j are reliable for all K algorithms over the N datasets, i.e.,

for each dataset, they are computed starting from the same random sample for all the algorithms.

In the following, the goal is to compare, using statistical hypothesis testing, algorithms respectively based/not based on the use of geometric patterns for univariate time series forecasting. These employ functions, respectively, of the form (1) and (2).

4. Proposed Time-Geometric Framework

This section introduces the Time-Geometric model, a novel approach that effectively extracts and exploits both temporal and geometric patterns for univariate time series forecasting. Figure 1 illustrates the general architecture of the model.

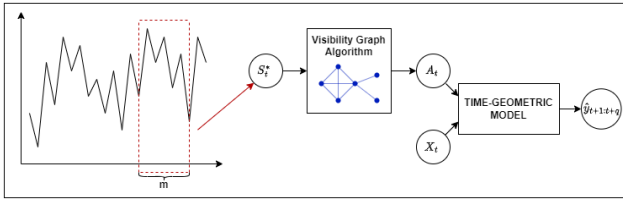


Figure 1. General idea of the proposed Time-Geometric Model.

Initially, we begin with the set S_t^* of the last m observations of our target time series S^* . Subsequently, we employ the visibility graph algorithm to derive a graph-based representation of the time series, encoded using the adjacency matrix A_t ¹. Finally, the Time-Geometric model receives the adjacency matrix A_t and the feature matrix X_t as inputs. Thus, the Time-Geometric model corresponds to the mapping function defined in Equation (1).

4.1. Visibility Graph Algorithm

We opt for the visibility graph algorithm (Lacasa et al., 2008) to construct the graph-based representation of the target time series S^* . This algorithm is chosen due to its capability to capture non-linear dependencies and patterns within time series data while preserving their structural properties. Depending on the nature of the time series — periodic, random, or fractal — we derive a regular graph, a random graph, or a small-world graph, respectively² (Lacasa et al., 2008). The resulting graph representation is connected and invariant to affine transformations of the time series (Stephen et al., 2015). Consider the target univariate time series $S^* = \{s_1^*, s_2^*, \dots, s_T^*\}$ associated with the set of discrete time steps $\mathcal{T} = \{1, 2, \dots, T\}$. The visibility graph algorithm represents the values of S^* as vertical bins, forming edges whenever there is a clear line of sight be-

tween two data points. This implies that an edge is formed between each pair of bars if the top of one bar is visible from the other. Each data point becomes a node in the graph, with edges representing visibility connections. The visibility condition, as defined in Lacasa et al. (2008), states that two data points (s_i^*, i) and (s_j^*, j) are connected if any other data point (s_k^*, k) satisfies: $s_k^* < s_j^* + (s_j^* - s_i^*) \frac{j-k}{j-i}$. This condition allows us to derive an undirected graph by considering all possible combinations of values for $i \in \{1, \dots, T\}$. Alternatively, we can obtain a directed graph by enforcing the “left-to-right” condition, comparing (s_j^*, j) only with data points where $k > i$, i.e., $\forall (s_j^*, j)$ with $j = i + 1, \dots, T$. The choice between a directed or undirected graph is an optimization hyperparameter. In Figure 2, we illustrate the steps of the visibility graph algorithm in obtaining the graph representation. The first plot displays the time series path, the middle plot illustrates the visibility condition and the link formation, and the final plot depicts the resulting undirected graph. The visibility graph can be computed for any length of the time series. However, in our model, we compute the graph representation considering the last m observations. Therefore, the associated adjacency matrix A_t has dimensions $m \times m$, with each node corresponding to a time observation.

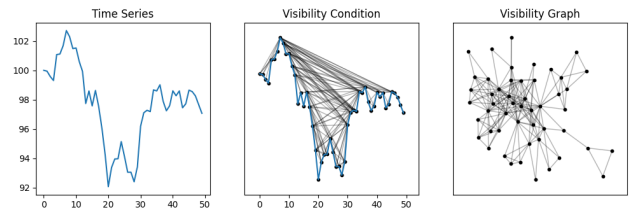


Figure 2. The Visibility Graph algorithm was applied to a time series generated from a Geometric Brownian Motion with the initial value equal to 100 and with mean and variance equal to 0.05 and 0.5, respectively. The computation of the algorithm was conducted using the “time series to visibility graphs” (ts2vg) Python package (Bergillos, 2020).

4.2. Time-Geometric Model

The Time-Geometric model receives input in the form of the adjacency matrix $A_t \in \mathbb{R}^{m \times m}$ and the feature matrix $X_t \in \mathbb{R}^{m \times F}$, where m represents the number of past observations considered, and F denotes the number of features. The model produces an output vector comprising q elements, denoted as $\hat{y}_{t+1:t+q}$.

As illustrated in Figure 3, the Time-Geometric model is comprised of three distinct components: the Time Component, the Geometric Component, and the Fully Connected Component.

¹Definition provided in Appendix B.1.

²Definitions provided in Appendix B.1.

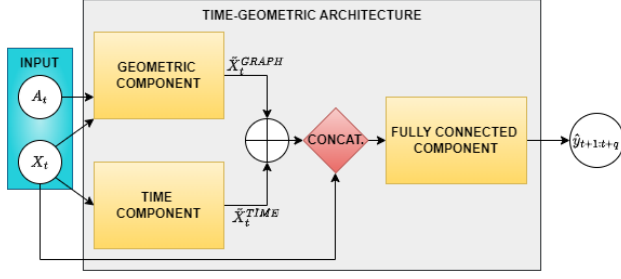


Figure 3. Time-Geometric Model Architecture. The baseline model differs in the absence of both the input A_t and the Geometric Component.

TIME COMPONENT

The Time Component takes the feature matrix $X_t \in \mathbb{R}^{m \times F'}$ as input and produces the output $\tilde{X}_t^{TIME} \in \mathbb{R}^{m \times F'}$. Its objective is to analyze and leverage temporal patterns within the data. Algorithm 1 outlines the operations of this component.

Algorithm 1 Time Component

Input: feature matrix X_t
Output: temporal pattern \tilde{X}_t^{TIME}
 $R_t^{(0)} = X_t$
for $l = 1$ **to** L **do**
 $R_t^{(l)} = \text{TIME}^{(l)}(R_t^{(l-1)})$
end for
 $\tilde{X}_t^{TIME} = \text{FC}(R_t^{(L)})$

The process involves initializing a hidden layer, denoted as $R_t^{(0)}$, with the feature matrix. Subsequently, based on the number of layers L , the l -th hidden layer of a neural network model for time series - $R_t^{(l)} = \text{TIME}^{(l)}(R_t^{(l-1)})$ - is applied. Here, $\text{TIME}^{(l)}$ represents the considered neural network model, akin to the mapping function $g(\cdot)$ defined in Equation (2). Specifically, for the Time Component analysis, the following neural network models are considered: Long Short-Term Memory (LSTM) (Hochreiter & Schmidhuber, 1997), Gated Recurrent Unit (GRU) (Chung et al., 2014), RNNs (Goodfellow et al., 2016), Bidirectional RNNs (BiRNNs) (Schuster & Paliwal, 1997), Bidirectional LSTM (BiLSTM) (Graves et al., 2005), Bidirectional GRU (BiGRU) (Xiong et al., 2016), Transformers (Vaswani et al., 2017), and TCNs (Lea et al., 2016). Finally, to obtain the output of the Time Component, a fully connected layer denoted as $\text{FC}(\cdot)$, is applied, defined by:

$$\tilde{X}_t^{TIME} = \phi \left(W_t R_t^{(L)} + b_t \right), \quad (3)$$

where W_t is the weight matrix, b is a bias vector, and $\phi(\cdot)$

denotes the activation function, a hyperparameter to be determined.

GEOMETRIC COMPONENT

The Geometric Component takes as input the adjacency matrix $A_t \in \mathbb{R}^{m \times m}$, derived using the visibility graph on the set S_t^* of the last m observations of the target time series S^* , and the feature matrix $X_t \in \mathbb{R}^{m \times F'}$. The output of this block represents the geometric patterns and is denoted as $\tilde{X}_t^{GRAPH} \in \mathbb{R}^{m \times F'}$. Algorithm 2 outlines the operations of this component.

Algorithm 2 Geometric Component

Input: adjacency matrix A_t , feature matrix X_t
Output: geometric pattern \tilde{X}_t^{GRAPH}
 $H_t^{(0)} = X_t$
for $l = 1$ **to** L' **do**
 $H_t^{(l)} = \text{GNN}^{(l)}(H_t^{(l-1)})$
end for
 $\tilde{X}_t^{GRAPH} = \text{LSTM}(H_t^{(L')})$

The process begins by initializing the hidden layer, denoted as $H_t^{(0)}$, with the feature matrix. Depending on the number of layers L' , the l -th layer of a GNN is applied, denoted as $H_t^{(l)} = \text{GNN}^{(l)}(H_t^{(l-1)})$. This can be defined using the message-passing paradigm:

$$M_{u \rightarrow v, t}^{(l)} = \text{MSG}^{(l)} \left(H_{u, t}^{(l-1)}, H_{v, t}^{(l-1)} \right),$$

$$H_{v, t}^{(l)} = \text{AGG}^{(l)} \left(M_{u \rightarrow v, t}^{(l)} | u \in N(v), H_{v, t}^{(l-1)} \right), \quad (4)$$

where $\text{MSG}^{(l)}(\cdot)$ represents the message function bringing the message embedding at the l -th layer, $N(v)$ represents the neighborhood of node v , and $\text{AGG}^{(l)}(\cdot)$ is the aggregation function that combines the messages received from neighboring nodes. The role of the message function is to facilitate the exchange of information among nodes and their neighbors (Hamilton et al., 2017). The notation “ l -th layer” denotes information originating from nodes that are at a distance of l -hops away. Note that changing the definition of the message and aggregation function, as defined in Equation (4), leads to different types of GNN models. In this research, we decide to consider only the Graph Convolutional Networks (GCNs) (Kipf & Welling, 2016), and the l -th layer can be defined as:

$$H_t^{(l)} = \rho \left(\tilde{D}_t^{-1/2} \tilde{A}_t \tilde{D}_t^{-1/2} H_t^{(l-1)} \Theta \right),$$

where $\rho(\cdot)$ is the activation function, Θ is the weight matrix, $\tilde{A}_t = A_t + I$, I is the identity matrix, \tilde{D}_t is the degree matrix computed on \tilde{A}_t . Before obtaining the output of the geometric component, we pass $H_t^{(L')}$ through an LSTM layer to process the geometric patterns.

FULLY CONNECTED COMPONENT

The inputs of the Fully Connected Component are the temporal patterns $\tilde{X}_t^{TIME} \in \mathbb{R}^{m \times F'}$, obtained from the Time Component, the geometric patterns $\tilde{X}_t^{GRAPH} \in \mathbb{R}^{m \times F'}$, computed by the Geometric Component, and the feature matrix $X_t \in \mathbb{R}^{m \times F'}$. Algorithm 3 outlines the operations of this component.

Algorithm 3 Fully Connected Component

Input: temporal pattern \tilde{X}_t^{TIME} , geometric pattern \tilde{X}_t^{GRAPH} , feature matrix X_t
Output: prediction $\hat{y}_{t+1:t+q}$
 $\tilde{X}_t^{TOT} = \tilde{X}_t^{TIME} + \tilde{X}_t^{GRAPH}$
if Skip Layer True **then**
 $\tilde{X}_t^{TOT} = \text{CONCAT}(\tilde{X}_t^{TOT}, X_t)$
end if
 $Z_t^{(0)} = \tilde{X}_t^{TOT}$
for $l = 1$ **to** L'' **do**
 $Z_t^{(l)} = \phi(\text{FC}^{(l)}(Z_t^{(l-1)}))$
end for
 $\hat{y}_{t+1:t+q} = Z_t^{(L'')}$

The process begins by summing up the two patterns, and the result is denoted as \tilde{X}_t^{TOT} . Then, if a skip layer is considered, \tilde{X}_t^{TOT} is concatenated with the feature matrix X_t . Finally, the hidden layer, denoted as $Z_t^{(0)}$ is initialized with \tilde{X}_t^{TOT} . Before obtaining the prediction vector, denoted as $\hat{y}_{t+1:t+q}$, the l -th layer of a fully connected model is applied, with the number of layers denoted as L'' .

5. Experimental Evaluation

In this section, we delineate the methodology employed for comparing the Time-Geometric model with the baseline model. We initiate by specifying the dataset and the pre-processing steps taken into account. Subsequently, we introduce the chosen evaluation metrics designed to facilitate the comparison. Prior to presenting the results, we expound on the process of determining the hyperparameters of the model utilized in the analysis. The computations were performed using the Nvidia GPU A100-SXM4-40GB.

5.1. Dataset, Pre-processing, and Evaluation Metrics

For our analysis, we focus on the constituents of the Standard & Poor 100 (S&P100), which exclusively includes the large-cap companies of the Standard & Poor 500. We gather daily observations of Close, Open, High, Low, and Volume for each stock from Yahoo Finance covering the period from January 04, 2015, to June 04, 2023. After excluding stocks with missing values, we obtain a dataset comprising 90 time series, each with 5 features, and approximately 2, 117 ob-

servations. Before normalizing each time series to achieve a mean of zero and a variance of one using a rolling window approach, we partition our dataset into training, validation, and test sets using the 0.6 – 0.2 – 0.2 rule.

To compare results across different models, we consider the following evaluation metrics: Root Mean Square Error (RMSE), Mean Absolute Percentage Error (MAPE), and Mean Absolute Scaled Error (MASE) (Hyndman & Koehler, 2006). A detailed exposition of the pre-processing steps and the evaluation metrics is provided in Appendix B.2 and B.3, respectively.

5.2. Configuration of the Models

To efficiently train our model, it is crucial to define the hyperparameters and the considered optimization strategy. The baseline models are the neural networks used in the Time Component, namely LSTM, RNN, GRU, BiLSTM, BiRNN, BiGRU, Transformers, TCN; these baseline models correspond to Equation (2). The Time-Geometric model involves combining the baseline models with GCN, corresponding to Equation (1). The hyperparameters to optimize encompass the batch size, sequence length (m), whether the dropout layer and skip connection are considered, and for both the Temporal and Geometric Components: the number of layers, L and L' respectively, the number of neurons, the dropout rate, and the activation function, $\phi(\cdot)$ and $\rho(\cdot)$ respectively. Moreover, in the Geometric Component, we also need to determine the hidden dimension of the LSTM layer and the direction of the graph. In the Fully Connected Component, the sole hyperparameter is the activation function $\phi(\cdot)$, as the number of layers was set to four with 128, 64, 32, 16 neurons respectively. The optimization of hyperparameters was performed using the Optuna Python package (Akiba et al., 2019), the Adam algorithm (Kingma & Ba, 2014) served as our optimization algorithm, and the Mean Squared Error (MSE) with the l_2 regularization term was used as loss function. Additionally, we specified the number of epochs as 1, 000 and incorporated early stopping with a patience of 20 epochs to mitigate the risk of overfitting. To optimize the hyperparameters, we employed an incremental optimization strategy. Initially, we optimized the hyperparameters for the baseline models. Subsequently, for the Time-Geometric model, we used the optimized hyperparameters of the baseline model for the Time Component and optimized only the hyperparameters for the Geometric Component. For more details on the hyperparameter optimization and their values, refer to Appendix C.

5.3. Numerical Results

We choose to forecast the ‘Close’ price variable, denoted as S^* , and conduct predictions at various temporal intervals denoted as q : daily, weekly, and monthly, corresponding to 1, 5, and 20 days. Furthermore, our feature matrix incorpo-

rates the variables ‘Close, High, Low, Open, and Volume’ for each stock considered.

In Figure 4 and Table 1, we present the comparison for the different evaluation metrics considered between our proposed model and the baseline model. Lower values indicate better model performance.

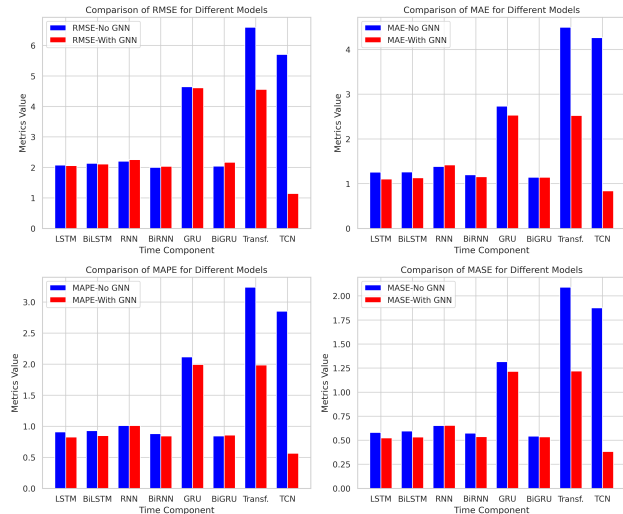


Figure 4. Average metric values for 1 day prediction for all the models within the considered dataset are presented in the figure. The x-axis denotes the models used both as baselines and in the Time Component. The blue bar represents the average metric values for the respective baseline model, while the red bar signifies the average metric value for the Time-Geometric model.

Table 1. The table displays the average metric values for a 1 day prediction across all models in the considered dataset. In parentheses, we specify the Time Component considered in the Time-Geometric model, denoted in the table as TG. The best-performing model for each metric is highlighted in bold.

MODEL	RMSE	MAE	MAPE	MASE
LSTM	2.0743	1.2570	0.9074	0.5810
BiLSTM	2.1349	1.2596	0.9276	0.5957
RNN	2.2012	1.3841	1.0110	0.6520
BiRNN	2.0006	1.1962	0.8797	0.5734
GRU	4.6464	2.7335	2.1174	1.3166
BiGRU	2.0438	1.1416	0.8441	0.5422
TRANSF.	6.5977	4.4957	3.2390	2.0907
TCN	5.7037	4.2612	2.8537	1.8767
TG(LSTM)	2.0580	1.1044	0.8262	0.5248
TG(BiLSTM)	2.1141	1.1311	0.8487	0.5338
TG(RNN)	2.2554	1.4192	1.0122	0.6553
TG(BiRNN)	2.0386	1.1529	0.8419	0.5377
TG(GRU)	4.6131	2.5326	1.9950	1.2150
TG(BiGRU)	2.1665	1.1420	0.8570	0.5360
TG(TRANSF.)	4.5617	2.5229	1.9869	1.2190
TG(TCN)	1.1420	0.8376	0.5658	0.3828

For ease of comparison, we compute the average for each considered metric across the dataset for each model. In Figure 4, the results for all the considered models are reported, both with the incorporation of GNN (our proposed framework) and without (baseline models). Notably, the impact of geometric patterns becomes evident only when the Time-Geometric model employs the Transformer and the RCN models for the Time Component, showcasing a noticeable improvement in average performance. In general, the use of a GNN slightly enhances the performance of the baseline model. This holds for several metrics. Such a trend persists when considering predictions at 5 and 20 days, as depicted in Figures 7 and 8, along with Tables 10 and 11 in Appendix D.1.

6. Statistical Significance of the Inclusion of the Geometric Patterns

In this section, we aim to demonstrate the statistical significance of the inclusion of geometric patterns in enhancing time series forecasting. We initiate this analysis by applying various pairwise test statistics to the metric results. Subsequently, we conduct multiple comparisons to reinforce and validate the robustness of the pairwise comparisons.

Recalling the notation introduced in Section 3, let K denote the number of algorithms compared, N represents the number of datasets used, and v_u^j indicate the evaluation metric of the j -th algorithm on the u -th dataset. In this research, we have compared 16 algorithms across 90 datasets, denoted by K and N , respectively. For both types of tests, we set the significance level, denoted by α , equal to 5%. This signifies our willingness to accept a 5% risk of erroneously concluding that there is a significant effect or difference when, in reality, there is none (Type I error).

6.1. Pairwise Comparison

In the pairwise comparison, we systematically assess the evaluation metrics for each baseline model and its corresponding Time-Geometric implementation (i.e., incorporating the Geometric Component) across multiple datasets. This involves scrutinizing the four metrics used to validate the improvement in the performance of the Time-Geometric model compared to its baseline model counterpart.

The null hypothesis for the pairwise comparison posits that the baseline and its Time-Geometric implementation perform equally well. Let $v_u^{j(BL)}$ denote the evaluation metric of the baseline model (denoted by $j(BL)$) on the u -th dataset, and $v_u^{j(TG)}$ denote the evaluation metric of the Time-Geometric inclusion (denoted by $j(TG)$) in the baseline model on the same dataset u . The null hypothesis is expressed as:

$$H_0 : v_u^{j(BL)} = v_u^{j(TG)}. \tag{5}$$

Table 2. The table presents the outcomes of the tests, with Acceptance denoted as A and Rejection as R . The test statistics for the Paired t-test, Wilcoxon test, and Sign test are encapsulated in brackets. The entry Δ -“Model” signifies the comparison between the baseline model and its corresponding Time-Geometric model. For the Paired t-test, we consider 89 degrees of freedom, resulting in a critical value of 1.986. In the Wilcoxon test, the critical value is 1.9599, and for the Sign test, the critical value is 54.42.

MODEL	PAIRED T-TEST				WILCOXON TEST				SIGN TEST			
	RMSE	MAE	MAPE	MASE	RMSE	MAE	MAPE	MASE	RMSE	MAE	MAPE	MASE
Δ LSTM	A(0.4)	R(4.1)	R(4.6)	R(5.1)	A(1.2)	R(4.4)	R(4.5)	R(4.2)	A(50)	R(64)	R(64)	R(65)
Δ BiLSTM	A(0.4)	R(4.0)	R(4.9)	R(6.7)	A(1.6)	R(5.9)	R(5.9)	R(5.6)	A(58)	R(73)	R(73)	R(73)
Δ RNN	A(0.8)	A(0.5)	A(.03)	A(0.1)	A(0.2)	A(.03)	A(.04)	A(.05)	A(46)	A(47)	A(47)	A(47)
Δ BiRNN	A(1.0)	A(1.0)	A(1.9)	R(2.6)	A(0.7)	A(1.9)	R(2.3)	R(2.0)	A(40)	A(53)	A(53)	A(50)
Δ GRU	A(1.7)	R(6.1)	R(8.9)	R(8.8)	A(1.3)	R(7.5)	R(7.5)	R(7.3)	A(47)	R(82)	R(82)	R(80)
Δ BiGRU	R(2.7)	A(.01)	A(0.7)	A(0.6)	R(3.9)	R(2.3)	A(1.9)	A(1.3)	R(60)	A(54)	A(54)	A(53)
Δ TRANSF.	R(4.8)	R(7.0)	R(12)	R(17)	R(8.2)	R(8.2)	R(8.2)	R(8.2)	R(90)	R(90)	R(90)	R(90)
Δ TCN	R(7.8)	R(8.2)	R(13)	R(20)	R(8.2)	R(8.2)	R(8.2)	R(8.2)	R(90)	R(90)	R(90)	R(90)

To analyze this null hypothesis, three different tests are considered: the Paired t-test, the Wilcoxon signed-ranks test (Wilcoxon, 1992), and the Sign test (Salzberg, 1997; Sheskin, 2003).

Paired t-test. This test examines whether the average difference in the evaluation metric between $v_u^{j(BL)}$ and $v_u^{j(TG)}$ is significantly different from zero. Let $d_u = v_u^{j(BL)} - v_u^{j(TG)}$ be the difference for the u -th dataset between the $j(BL)$ and $j(TG)$ algorithms, and $\bar{d} = \frac{1}{N} \sum_{u=1}^N d_u$ be the average difference. The null hypothesis, defined in Equation (5), can be expressed as: $\mathbf{H}_0 : \mu_d = 0$, where μ_d represent the true mean that is approximated with the sample mean, i.e., \bar{d} . Finally, the Paired t-test statistic is computed as: $z^t = \frac{\bar{d}}{\sigma_{\bar{d}}}$, where $\sigma_{\bar{d}}$ represents the standard deviation of the average difference, and z^t follows a Student distribution with $N - 1$ degrees of freedom.

Wilcoxon signed-ranks test. This non-parametric test ranks the differences d_i for the two algorithms for each dataset N , ignoring the signs, and then compares the ranks for positive and negative differences. The Wilcoxon test is a more robust alternative to the Paired t-test, assuming commensurability of the differences. Let B^+ denote the sum of the ranks for which the $j(TG)$ algorithm performs better than the $j(BL)$ algorithm (i.e., $v_u^{j(TG)} < v_u^{j(BL)}$), and let B^- represent the opposite case. The Wilcoxon statistic is then defined as:

$$z^w = \frac{B^* - \frac{1}{4}N(N+1)}{\sqrt{\frac{1}{24}N(N+1)(2N+1)}}$$

where $B^* = \min(B^+, B^-)$, and z^w follows a normal distribution for large numbers of datasets.

Sign test. In the Sign test, we count the total number of times that the algorithm $j(TG)$ outperforms $j(BL)$, denoted by $|\#W|$ (i.e., $v_u^{j(TG)} < v_u^{j(BL)}$). Under the null hypothesis, each algorithm should outperform the other approximately $N/2$ times. We can rewrite Equation (5) as $\mathbf{H}_0 : p\{v_u^{j(TG)} < v_u^{j(BL)}\} = 0.5$, with $p\{\cdot\}$ denoting

probability. For $N > 25$, $|\#W|$ is approximately distributed following a normal distribution with mean $\frac{N}{2}$ and variance $\frac{\sqrt{N}}{2}$. The difference in performance between algorithms $j(TG)$ and $j(BL)$ is statistically significant if: $|\#W| \geq \frac{N}{2} + 1.96 \frac{\sqrt{N}}{2}$, where 1.96 is the critical value for a normal distribution at the 95% confidence interval.

In Table 2, we present the results of the test statistics for the evaluation metrics considered in the context of the 1 day prediction. Entries marked with A signify acceptance of the null hypothesis, while those marked with R indicate rejection, and the corresponding statistical test values are enclosed in parentheses. Additionally, Δ -“Model” denotes the comparison between the baseline model and its counterpart incorporating GCNs. Results for the 5 day and 20 day predictions are detailed in Tables 12 and 13, respectively, available in Appendix E.1. Observing Table 2, it becomes apparent that the statistical significance of the models is notably contingent on the choice of evaluation metrics. Specifically, only Δ -Tranf., Δ -TCN, and Δ -RNN exhibit consistent statistical outcomes across all metrics. This suggests that the statistical significance of the inclusion of geometric patterns, and more broadly, the distinctions among the models, is influenced by the specific evaluation metrics employed. These observations persist for the 5 day and 20 day tests, as shown in Tables 12 and 13, respectively, in Appendix E.1. In the case of the 5 day test statistics, there is a more uniform trend in the results. This indicates that the prediction horizon also plays a crucial role in determining the statistical significance of a model relative to others.

6.2. Multiple Comparison

Relying solely on pairwise comparisons for each algorithm and its Time-Geometric implementation could potentially lead to the random rejection of the considered null hypothesis. To mitigate this, we also execute a multiple comparison, aimed at controlling the probability of making a Type I error in at least one individual comparison, commonly referred to

Table 3. The table displays the Friedman test results for each metric considered, with Acceptance denoted as A and Rejection as R , while the test statistics are reported in brackets. We consider 15 degrees of freedom, resulting in a critical value of 27.48.

METRIC	1-DAY	5-DAY	20-DAY
RMSE	R(1041)	R(1068)	R(654)
MAE	R(1025)	R(1034)	R(652)
MAPE	R(1025)	R(1034)	R(652)
MASE	R(1025)	R(1040)	R(653)

as “family-wise error” (Demšar, 2006).

In the multiple comparison, we analyze all the algorithms together for each dataset, considering one evaluation metric at a time. Specifically, the multiple comparison is executed using the Friedman test (Friedman, 1937; 1940), where we rank the performance v_u^j of each algorithm for each dataset. We sort the selected evaluation metric in increasing order, assigning a rank of 1 to the first element, 2 to the second, and so forth. Let RK_u^j define the rank of the j -th algorithm on the u -th dataset for the selected metric. The Friedman test analyzes the average ranks of the algorithms, computed as $\bar{RK}_j = \frac{1}{N} \sum_{u=1}^N RK_u^j$. The average ranks for each algorithm, each evaluation metric, and each forecasting horizon are reported in Table 14 in Appendix E.2. The null hypothesis posits that all the algorithms are equivalent, implying their ranks are also equivalent. Thus, the Friedman test checks if the average ranks are statistically different from the mean among all the ranks. The Friedman statistic is computed as:

$$\chi_F^2 = \frac{12N}{K(K+1)} \left[\sum_{j=1}^K \bar{RK}_j^2 - \frac{K(K+1)^2}{4} \right],$$

where χ_F^2 follows a Chi-squared distribution with $K - 1$ degrees of freedom when $N > 10$ and $K > 5$. The outcome of the Friedman test is reported in Table 3. Observing Table 3, the null hypothesis of the Friedman test is always rejected for each metric and each forecasting horizon considered, meaning that there exists a difference in the performance among the algorithms. In order to study such a difference, we can perform the Nemenyi test (Nemenyi, 1963), where we compare all the algorithms to each other. Specifically, we state that the difference in performance of two algorithms is statistically significant if their average rank difference is at least larger than a critical difference, denoted by $CD = q_\alpha \sqrt{\frac{K(K+1)}{6N}}$, where q_α is a critical value derived from the Standardized Range statistics and divided by $\sqrt{2}$ (Demšar, 2006). Substituting the corresponding value into the equation for the critical value, we determine that CD is set at 2.50. Figure 5 presents the results of the Nemenyi test for all the evaluation metrics considered in the context of a 1 day forecasting horizon. The comparative

Nemenyi Test for Evaluation Metrics with 1 day forecasting horizon

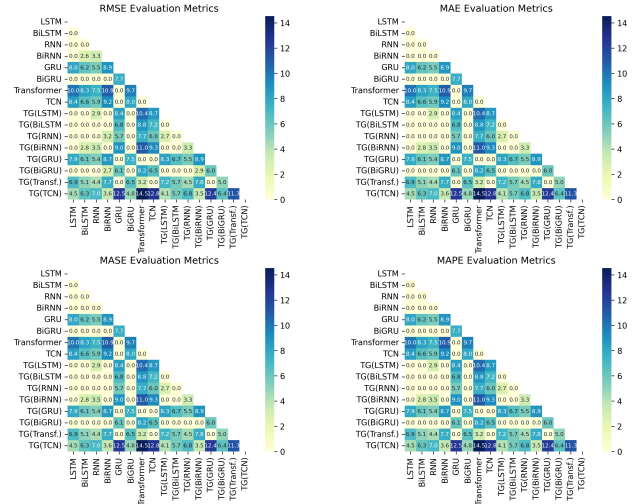


Figure 5. Nemenyi test for 1 day forecasting. Non-statistically significant relationships are highlighted in yellow.

analysis for the 5 day and 20 day predictions is detailed in Figure 9 and 10 in Appendix E.2, respectively. In all figures, non-statistically significant results are highlighted in yellow. Upon scrutinizing the ranks across models for each evaluation metric, we arrive at a conclusion consistent with the pairwise comparison. The choice of evaluation metrics and the forecasting horizon significantly influence the determination of a model’s statistical significance. Notably, the Time-Geometric model underscores the statistical relevance of geometric patterns in enhancing the predictive accuracy of the baseline model.

7. Conclusion

In this study, we introduce the Time-Geometric model designed to leverage both temporal and geometric patterns for univariate financial time series forecasting. This is accomplished by integrating Graph Convolutional Networks into the baseline neural network model for time series, where the graph representation is derived from the visibility graph. We assess the performance of our model in comparison to various baseline models using a dataset comprising 90 financial time series. Subsequently, we demonstrate that the statistical significance observed among the models is contingent on the choice of evaluation metric and forecasting horizon. Furthermore, we uncover the statistical significance of incorporating geometric patterns in enhancing forecasting accuracy. Future research endeavors will concentrate on elucidating the behavior of evaluation metrics and exploring the statistical significance of the inclusion of geometric patterns across diverse time series datasets.

References

- Akiba, T., Sano, S., Yanase, T., Ohta, T., and Koyama, M. Optuna: A next-generation hyperparameter optimization framework. In *Proceedings of the 25th ACM SIGKDD International Conference on Knowledge Discovery & Data Mining*, pp. 2623–2631, 2019.
- Ariyo, A. A., Adewumi, A. O., and Ayo, C. K. Stock price prediction using the ARIMA model. In *2014 UKSim-AMSS 16th International Conference on Computer Modelling and Simulation*, pp. 106–112. IEEE, 2014.
- Barabási, A.-L. Network science. *Philosophical Transactions of the Royal Society A: Mathematical, Physical and Engineering Sciences*, 371(1987):20120375, 2013.
- Barrera-Animas, A. Y., Oyedele, L. O., Bilal, M., Akinosho, T. D., Delgado, J. M. D., and Akanbi, L. A. Rainfall prediction: A comparative analysis of modern machine learning algorithms for time-series forecasting. *Machine Learning with Applications*, 7:100204, 2022.
- Benidis, K., Rangapuram, S. S., Flunkert, V., Wang, Y., Maddix, D., Turkmen, C., Gasthaus, J., Bohlke-Schneider, M., Salinas, D., Stella, L., et al. Deep learning for time series forecasting: Tutorial and literature survey. *ACM Computing Surveys*, 55(6):1–36, 2022.
- Bergillos, C. Ts2vg: Time series to visibility graphs. <https://pypi.org/project/ts2vg/>, 2020. Accessed: 2023-08-09.
- Bishop, C. M. *Pattern Recognition and Machine Learning*. Springer New York, NY, 1 edition, 2016.
- Black, F. and Scholes, M. The pricing of options and corporate liabilities. *Journal of Political Economy*, 81(3): 637–654, 1973.
- Bollerslev, T., Engle, R. F., and Nelson, D. B. ARCH models. *Handbook of Econometrics*, 4:2959–3038, 1994.
- Box, G. E., Jenkins, G. M., Reinsel, G. C., and Ljung, G. M. *Time Series Analysis: Forecasting and Control*. John Wiley & Sons, 5 edition, 2015.
- Brockwell, P. J. and Davis, R. A. *Time Series: Theory and Methods*. Springer Science & Business Media, 1991.
- Cao, D., Wang, Y., Duan, J., Zhang, C., Zhu, X., Huang, C., Tong, Y., Xu, B., Bai, J., Tong, J., et al. Spectral temporal graph neural network for multivariate time-series forecasting. *Advances in Neural Information Processing Systems*, 33:17766–17778, 2020.
- Chen, C., Xue, L., and Xing, W. Research on improved GRU-based stock price prediction method. *Applied Sciences*, 13(15):8813, 2023.
- Cheng, D., Yang, F., Xiang, S., and Liu, J. Financial time series forecasting with multi-modality graph neural network. *Pattern Recognition*, 121:108218, 2022. ISSN 0031-3203. doi: <https://doi.org/10.1016/j.patcog.2021.108218>. URL <https://www.sciencedirect.com/science/article/pii/S003132032100399X>.
- Chung, J., Gulcehre, C., Cho, K., and Bengio, Y. Empirical evaluation of gated recurrent neural networks on sequence modeling. *arXiv preprint arXiv:1412.3555*, 2014.
- Demšar, J. Statistical comparisons of classifiers over multiple data sets. *The Journal of Machine Learning Research*, 7:1–30, 2006.
- Ding, Q., Wu, S., Sun, H., Guo, J., and Guo, J. Hierarchical multi-scale Gaussian transformer for stock movement prediction. In Bessiere, C. (ed.), *Proceedings of the Twenty-Ninth International Joint Conference on Artificial Intelligence, IJCAI-20*, pp. 4640–4646. International Joint Conferences on Artificial Intelligence Organization, 7 2020. doi: 10.24963/ijcai.2020/640. URL <https://doi.org/10.24963/ijcai.2020/640>. Special Track on AI in FinTech.
- Elman, J. L. Finding structure in time. *Cognitive Science*, 14(2):179–211, 1990.
- Engle, R. F. Autoregressive conditional heteroscedasticity with estimates of the variance of united kingdom inflation. *Econometrica: Journal of the Econometric Society*, pp. 987–1007, 1982.
- Francq, C. and Zakoian, J.-M. *GARCH models: Structure, Statistical Inference and Financial Applications*. John Wiley & Sons, 2019.
- Friedman, M. The use of ranks to avoid the assumption of normality implicit in the analysis of variance. *Journal of the American Statistical Association*, 32(200):675–701, 1937.
- Friedman, M. A comparison of alternative tests of significance for the problem of m rankings. *The Annals of Mathematical Statistics*, 11(1):86–92, 1940.
- Ghosh, A., Bose, S., Maji, G., Debnath, N., and Sen, S. Stock price prediction using LSTM on Indian share market. In *Proceedings of the 32nd International Conference on n Computer Applications in Industry and Engineering*, volume 63, pp. 101–110, 2019.
- Goodfellow, I., Bengio, Y., and Courville, A. *Deep Learning*. MIT Press, 2016. <http://www.deeplearningbook.org>.

- Graves, A., Fernández, S., and Schmidhuber, J. Bidirectional LSTM networks for improved phoneme classification and recognition. In *International Conference on Artificial Neural Networks*, pp. 799–804. Springer, 2005.
- Guo, T., Xu, Z., Yao, X., Chen, H., Aberer, K., and Funaya, K. Robust online time series prediction with recurrent neural networks. In *2016 IEEE International Conference on Data Science and Advanced Analytics (DSAA)*, pp. 816–825. Ieee, 2016.
- Hamilton, J. D. *Time Series Analysis*. Princeton University Press, 2020.
- Hamilton, W., Ying, Z., and Leskovec, J. Inductive representation learning on large graphs. *Advances in Neural Information Processing Systems*, 30, 2017.
- Hochreiter, S. and Schmidhuber, J. Long short-term memory. *Neural Computation*, 9(8):1735–1780, 1997.
- Hua, Y., Zhao, Z., Li, R., Chen, X., Liu, Z., and Zhang, H. Deep learning with long short-term memory for time series prediction. *IEEE Communications Magazine*, 57(6):114–119, 2019.
- Hyndman, R. J. and Koehler, A. B. Another look at measures of forecast accuracy. *International Journal of Forecasting*, 22(4):679–688, 2006.
- Kingma, D. P. and Ba, J. Adam: A method for stochastic optimization. *arXiv preprint arXiv:1412.6980*, 2014.
- Kipf, T. N. and Welling, M. Semi-supervised classification with graph convolutional networks. *arXiv preprint arXiv:1609.02907*, 2016.
- Lacasa, L., Luque, B., Ballesteros, F., Luque, J., and Nuno, J. C. From time series to complex networks: The visibility graph. *Proceedings of the National Academy of Sciences*, 105(13):4972–4975, 2008.
- Lamberton, D. and Lapeyre, B. *Introduction to Stochastic Calculus Applied to Finance*. CRC press, 2011.
- Lazcano, A., Herrera, P. J., and Monge, M. A combined model based on recurrent neural networks and graph convolutional networks for financial time series forecasting. *Mathematics*, 11(1):224, 2023.
- Lea, C., Vidal, R., Reiter, A., and Hager, G. D. Temporal convolutional networks: A unified approach to action segmentation, 2016.
- Lee, S. K., Nguyen, L., and Sy, M. O. Comparative study of volatility forecasting models: The case of Malaysia, Indonesia, Hong Kong and Japan stock markets. *Economics*, 5(4):299–310, 2017.
- Lin, Y., Huang, Q., Zhong, Q., Li, M., Li, Y., and Ma, F. A new attention-based LSTM model for closing stock price prediction. *International Journal of Financial Engineering*, 9(03):2250014, 2022.
- Lu, W., Li, J., Wang, J., and Qin, L. A CNN-BiLSTM-AM method for stock price prediction. *Neural Computing and Applications*, 33:4741–4753, 2021.
- Mahalakshmi, G., Sridevi, S., and Rajaram, S. A survey on forecasting of time series data. In *2016 International Conference on Computing Technologies and Intelligent Data Engineering (ICCTIDE'16)*, pp. 1–8. IEEE, 2016.
- Mahmoud, A. and Mohammed, A. A survey on deep learning for time-series forecasting. *Machine Learning and Big Data Analytics Paradigms: Analysis, Applications and Challenges*, pp. 365–392, 2021.
- Mandelbrot, B. B. *Fractals and Scaling in Finance: Discontinuity, Concentration, Risk. Selecta volume E*. Springer Science & Business Media, 2013.
- Nemenyi, P. B. *Distribution-Free Multiple Comparisons*. Princeton University, 1963.
- Parmezan, A. R. S., Souza, V. M., and Batista, G. E. Evaluation of statistical and machine learning models for time series prediction: Identifying the state-of-the-art and the best conditions for the use of each model. *Information Sciences*, 484:302–337, 2019. ISSN 0020-0255. doi: <https://doi.org/10.1016/j.ins.2019.01.076>. URL <https://www.sciencedirect.com/science/article/pii/S0020025519300945>.
- Roondiwala, M., Patel, H., and Varma, S. Predicting stock prices using LSTM. *International Journal of Science and Research (IJSR)*, 6(4):1754–1756, 2017.
- Rounaghi, M. M. and Zadeh, F. N. Investigation of market efficiency and financial stability between S&P 500 and London stock exchange: Monthly and yearly forecasting of time series stock returns using ARMA model. *Physica A: Statistical Mechanics and its Applications*, 456:10–21, 2016.
- Ruiz, L., Gama, F., and Ribeiro, A. Gated graph recurrent neural networks. *IEEE Transactions on Signal Processing*, 68:6303–6318, 2020.
- Salzberg, S. L. On comparing classifiers: Pitfalls to avoid and a recommended approach. *Data Mining and Knowledge Discovery*, 1:317–328, 1997.
- Scarselli, F., Gori, M., Tsoi, A. C., Hagenbuchner, M., and Monfardini, G. The graph neural network model. *IEEE Transactions on Neural Networks*, 20(1):61–80, 2008.

- Schuster, M. and Paliwal, K. K. Bidirectional recurrent neural networks. *IEEE Transactions on Signal Processing*, 45(11):2673–2681, 1997.
- Selvin, S., Vinayakumar, R., Gopalakrishnan, E., Menon, V. K., and Soman, K. Stock price prediction using LSTM, RNN and CNN-sliding window model. In *2017 International Conference on Advances in Computing, Communications and Informatics (ICACCI)*, pp. 1643–1647. IEEE, 2017.
- Sheskin, D. J. *Handbook of Parametric and Nonparametric Statistical Procedures*. Chapman and hall/CRC, 2003.
- Shih, H. M. and Rajendran, S. Comparison of time series methods and machine learning algorithms for forecasting taiwan blood services foundation’s blood supply. *Journal of Healthcare Engineering*, 2019, 2019. URL <https://api.semanticscholar.org/CorpusID:203815441>.
- Stephen, M., Gu, C., and Yang, H. Visibility graph based time series analysis. *PloS One*, 10(11):e0143015, 2015.
- Tankov, P. and Cont, R. *Financial Modelling with Jump Processes*. CRC Press, 2003.
- Tsay, R. S. *Analysis of Financial Time Series*. John Wiley & Sons, 2005.
- Vaswani, A., Shazeer, N., Parmar, N., Uszkoreit, J., Jones, L., Gomez, A. N., Kaiser, L., and Polosukhin, I. Attention is all you need. *Advances in Neural Information Processing Systems*, 30, 2017.
- Wilcoxon, F. Individual comparisons by ranking methods. In *Breakthroughs in Statistics: Methodology and Distribution*, pp. 196–202. Springer, 1992.
- Wu, Z., Pan, S., Chen, F., Long, G., Zhang, C., and Yu, P. S. A comprehensive survey on graph neural networks. *IEEE Transactions on Neural Networks and Learning Systems*, 32(1):4–24, January 2021. ISSN 2162-2388. doi: 10.1109/tnnls.2020.2978386. URL <http://dx.doi.org/10.1109/TNNLS.2020.2978386>.
- Xiang, S., Cheng, D., Shang, C., Zhang, Y., and Liang, Y. Temporal and heterogeneous graph neural network for financial time series prediction. In *Proceedings of the 31st ACM International Conference on Information & Knowledge Management, CIKM ’22*, pp. 3584–3593, New York, NY, USA, 2022. Association for Computing Machinery. ISBN 9781450392365. doi: 10.1145/3511808.3557089. URL <https://doi.org/10.1145/3511808.3557089>.
- Xiong, C., Merity, S., and Socher, R. Dynamic memory networks for visual and textual question answering. In *International Conference on Machine Learning*, pp. 2397–2406. PMLR, 2016.
- Xu, B., Shen, H., Cao, Q., Qiu, Y., and Cheng, X. Graph wavelet neural network. In *International Conference on Learning Representations*, 2019. URL <https://openreview.net/forum?id=H1ewdiR5tQ>.
- You, J., Du, T., and Leskovec, J. Roland: graph learning framework for dynamic graphs. In *Proceedings of the 28th ACM SIGKDD Conference on Knowledge Discovery and Data Mining*, pp. 2358–2366, 2022.
- Yu, B., Yin, H., and Zhu, Z. Spatio-temporal graph convolutional networks: A deep learning framework for traffic forecasting. In *Proceedings of the Twenty-Seventh International Joint Conference on Artificial Intelligence, IJCAI-2018*. International Joint Conferences on Artificial Intelligence Organization, July 2018. doi: 10.24963/ijcai.2018/505. URL <http://dx.doi.org/10.24963/ijcai.2018/505>.
- Zhang, L., Aggarwal, C., and Qi, G.-J. Stock price prediction via discovering multi-frequency trading patterns. In *Proceedings of the 23rd ACM SIGKDD International Conference on Knowledge Discovery and Data Mining*, pp. 2141–2149, 2017.
- Zhao, G., Xue, M., and Cheng, L. A new hybrid model for multi-step WTI futures price forecasting based on self-attention mechanism and spatial-temporal graph neural network. *Resources Policy*, 85:103956, 2023. ISSN 0301-4207. doi: <https://doi.org/10.1016/j.resourpol.2023.103956>. URL <https://www.sciencedirect.com/science/article/pii/S0301420723006670>.
- Zhao, L., Song, Y., Zhang, C., Liu, Y., Wang, P., Lin, T., Deng, M., and Li, H. T-GCN: A temporal graph convolutional network for traffic prediction. *IEEE Transactions on Intelligent Transportation Systems*, 21(9): 3848–3858, September 2020. ISSN 1558-0016. doi: 10.1109/tits.2019.2935152. URL <http://dx.doi.org/10.1109/TITS.2019.2935152>.

A. Related work

Numerous studies have extensively explored diverse tasks related to time series, encompassing prediction and classification methodologies (Mahalakshmi et al., 2016; Mahmoud & Mohammed, 2021; Benidis et al., 2022). This section presents a comprehensive overview of both deep learning and statistical models as applied to the forecasting of univariate financial time series.

A.1. Time Series Forecasting with Statistical Models

Statistical models aim to discern and encapsulate distinct components within a time series, namely Trend, Seasonality, and Noise (Box et al., 2015). The AutoRegressive Moving Average (ARMA) model (Brockwell & Davis, 1991) serves as a foundational statistical model for univariate time series analysis, amalgamating autoregressive and moving average elements. In a study by Rounaghi & Zadeh (2016), the ARMA model was employed for predicting stock returns in both the Standard and Poor's 500 (S&P500) and the London Stock Exchange. However, limitations arise as the ARMA model assumes stationarity within the time series, presupposing constancy in mean and variance over time. The AutoRegressive Integrated Moving Average (ARIMA) model (Hamilton, 2020) extends the ARMA model by not explicitly assuming time series stationarity. Instead, the integrated component introduces differencing in the time series, achieving stationarity. Ariyo et al. (2014) applied the ARIMA model to predict the New York Stock Exchange (NYSE) and the Nigeria Stock Exchange (NSE). Nevertheless, the ARIMA model reveals its constraints when faced with non-constant variance over time. To address the challenge of evolving volatility, the AutoRegressive Conditional Heteroskedasticity (ARCH) model was introduced (Bollerslev et al., 1994). In a study by Engle (1982), the ARCH model was employed to estimate mean and variance in the United Kingdom from 1958 to 1977. However, the ARCH model assumes homoscedastic volatility changes, signifying constant variance. Mitigating this limitation, the Generalized AutoRegressive Conditional Heteroskedasticity (GARCH) model was proposed (Francq & Zakoian, 2019). Lee et al. (2017) conducted a comparative analysis between the ARIMA and GARCH models for predicting volatility in various stock exchanges.

A.2. Time Series Forecasting with Deep Learning Models

In contrast to statistical models, deep learning models offer the advantage of not requiring stationarity assumptions in time series data. Furthermore, they have demonstrated notable efficacy in capturing intricate non-linear patterns within such data. Among the class of neural network models tailored for time series analysis, Recurrent Neural Networks (RNNs) (Goodfellow et al., 2016) represent a fundamental model designed for sequential data processing. Guo et al. (2016) applied RNNs for time series forecasting within the domain of anomaly detection. However, RNNs face challenges associated with the vanishing gradient problem, limiting their ability to capture long-term relationships within a time series. To address this limitation, the Long Short-Term Memory (LSTM) (Hochreiter & Schmidhuber, 1997) model was introduced, along with its simplified counterpart, the Gated Recurrent Unit (GRU) (Chung et al., 2014). Ghosh et al. (2019) utilized LSTM for predicting Indian Stock Exchanges, while Chen et al. (2023) compared the GRU model with other machine learning models for stock price prediction across various industries. Additionally, Roondiwala et al. (2017) employed LSTM to predict the NIFTY50 index. Zhang et al. (2017) enhanced the LSTM model's performance by integrating the Discrete Fourier Transform into the memory cell. Furthermore, an attention mechanism was incorporated to augment the predictive capability of the LSTM model for various stock exchanges in Lin et al. (2022). Selvin et al. (2017) conducted a comparative analysis of the forecasting accuracy of LSTM, RNNs, and Convolutional Neural Networks (CNNs) on the Indian Stock Exchange. Finally, ensemble methods were proposed for predicting the Shanghai Composite index in Ding et al. (2020); Lu et al. (2021).

B. Preliminaries

This section offers a comprehensive discussion about the principles of Network Theory, the pre-processing stage, and the evaluation metrics considered in our study.

B.1. Network Theory

Let $G = (V, E)$ be a graph, where $V = \{v_1, \dots, v_n\}$ is the set of nodes, and $E \subseteq V \times V$ is the set of edges. The associated adjacency matrix A for the graph G is defined with entries a_{uv} as follows:

$$a_{uv} = \begin{cases} 1 & \text{if } (u, v) \in E, \\ 0 & \text{otherwise.} \end{cases}$$

This implies that nodes u and v are connected by an edge if and only if $a_{uv} = 1$. Notably, the adjacency matrix A is an $n \times n$ matrix.

Furthermore, a dynamic graph is conceptualized as a sequence of static graph snapshots indexed by discrete time. This approach, termed ‘‘snapshot-based representation’’ (You et al., 2022), defines a dynamic graph as $G = \{G_t\}_{t=1}^T$, where $G_t = (V_t, E_t)$ with $V_t \subseteq V$ and $E_t \subseteq E$. It is crucial to note that the set of nodes and edges may vary across different graph snapshot representations.

In this study, the visibility graph is employed to derive the graph representation of the time series. This algorithm is chosen for its capability to preserve the structural properties of time series data (Lacasa et al., 2008). Specifically, a periodic time series transforms into a regular graph, a random time series manifests as a random graph, and a fractal time series results in a small-world graph. The regular, random, and small-world graph properties are elucidated in Barabási (2013), together with related topological characteristics. In a regular graph, each node v has an identical number of connections, forming a highly ordered and structured network. This type of graph exhibits a regular and symmetrical pattern of connections, fostering uniformity throughout the network. Conversely, in a random graph, connections between nodes occur randomly, leading to a more unpredictable and less structured network. Here, v and u are connected with a probability p . Lastly, the small-world graph is characterized by the presence of a few hubs: some nodes possess a large number of links, while many nodes have only a few links. This entails that most nodes can be reached from every other node in a small number of steps, while still maintaining local clusters or neighborhoods. To determine whether a graph is a regular, random, or small-world graph, the degree distribution of the graph must be analyzed. The degree of a node in a graph, denoted k_u , measures how connected or central that node is within the network and is defined as $k_u = \sum_{v=1}^{|V|} a_{uv}$.

Figure 6 exemplifies the characteristics of the degree distribution in a regular graph, a random graph, and a small-world graph. The total number of nodes is fixed at 100, the degree for the regular graph is set to 30, the probability of connecting two nodes in the random graph is set to 0.2, and the small-world graph is configured with 10 nearest neighbors to connect and a rewiring probability of 0.1.

B.2. Pre-Processing

In this research, we gather data comprising the ‘‘Close, Open, High, Low’’ prices, and the Volume for each stock considered within the Standard & Poor 100 index. Normalization is employed to effectively capture non-linear patterns within the time series. To prevent potential data leakage during normalization, we adopt a rolling window approach. The dataset is normalized using the following method:

$$\bar{x}_t^i = \frac{x_t^i - \mu_t^i}{\sigma_t^i}.$$

Here, $i \in \{Close, Open, High, Low, Volume\}$, x_t^i represents the i -th feature’s value at time t , while μ_t^i and σ_t^i denote the mean and standard deviation, respectively, of feature i . These statistical measures are computed using a rolling window, the length of which is a hyperparameter subject to optimization.

B.3. Evaluation Metrics

The purpose of employing evaluation metrics is to facilitate a comparative analysis of forecasting accuracy among the models utilized in this study. Four evaluation metrics were chosen for consideration: Root Mean Square Error (RMSE), Mean Absolute Error (MAE), Mean Absolute Percentage Error (MAPE), and Mean Absolute Scaled Error (MASE). For a

Degree Distribution for a Regular, Random, and Small-World Graph

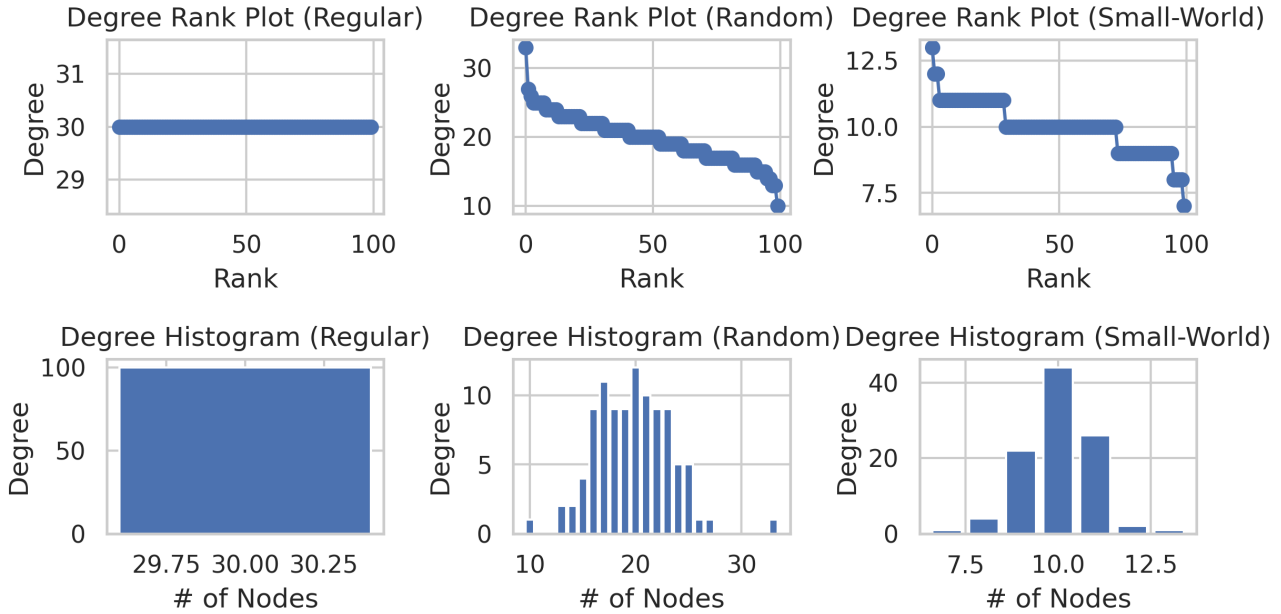


Figure 6. Example of degree distribution for a regular graph, a random graph, and a small-world graph.

dataset containing M elements, these evaluation metrics are defined as follows:

$$RMSE = \sqrt{\frac{1}{M} \sum_{i=1}^M (y_i - \hat{y}_i)^2},$$

$$MAE = \frac{1}{M} \sum_{i=1}^M |y_i - \hat{y}_i|,$$

$$MAPE = \frac{1}{M} \sum_{i=1}^M \left| \frac{y_i - \hat{y}_i}{y_i} \right|,$$

$$MASE = \frac{MAE}{\frac{1}{M-1} \sum_{i=2}^M |y_i - y_{i-1}|},$$

where y_i represents the true value for the i -th example, and \hat{y}_i is the prediction of the model. It is noteworthy that, for the evaluation metrics employed to gauge forecasting accuracy, smaller values indicate superior performance. Specifically, MASE was included in our selection due to its nature as a scale-free error metric. This implies that the MASE metric is less influenced by the scale of the data. Finally, the MASE metric compares the actual forecast against a naive forecast where the future one-step ahead value is set equal to the previous value. For the MASE metric, a value greater than 1 suggests that the naive forecast outperforms the model's forecast, while a value lower than 1 indicates the opposite.

C. Hyperparameters

This section outlines the hyperparameter optimization procedures implemented in the proposed analysis. Initially, we present the hyperparameters for the baseline models, followed by those for the Time-Geometric model.

For hyperparameter optimization, we employed the Python package Optuna (Akiba et al., 2019). Optuna facilitates optimization for a wide range of machine-learning models. Operating on the study-trial framework, Optuna defines a “study” as an optimization based on an objective function and a “trial” as a single execution of this optimization. The objective of a study is to identify the optimal set of hyperparameter values through multiple trials. We conducted 1000 trials for each considered model.

Lastly, it is important to highlight that the choice of the loss function, regularization term, and optimization algorithm, as detailed in Section 5, has been made a priori for computational efficiency considerations.

C.1. Baseline Models

In our analysis, we include the following baseline models: Long Short-Term Memory (LSTM), Bidirectional LSTM (BiLSTM), Recurrent Neural Network (RNN), Bidirectional RNN (BiRNN), Gated Recurrent Unit (GRU), Bidirectional GRU (BiGRU), Transformer, and Temporal Convolutional Network (TCN). The hyperparameters for these baseline neural network models encompass learning rate, number of neurons, number of layers, sequence length, batch size, dropout rate, and activation function. Tables 4, 5, and 6 present the detailed hyperparameters for the baseline models corresponding to prediction horizons of 1, 5, and 20 days.

Table 4. The table displays the hyperparameter values for a 1 day prediction and the baseline models considered.

HYPERPARAM.	LSTM	BiLSTM	RNN	BiRNN	GRU	BiGRU	TRANF.	TCN
LEARNING RATE	0.000176	0.000258	0.000985	0.000656	0.000405	0.000134	0.000883	0.000935
# NEURONS	190	140	110	30	120	30	-	200
# LAYERS	2	2	2	2	3	2	2	-
SEQUENCE LENGTH	100	100	100	100	100	100	100	100
BATCH SIZE	40	160	160	80	160	80	40	160
DROPOUT RATE	0.08	0.47	0.06	0.03	0.33	0.06	0.01	0.08
ACTIVATION FUNCTION	SELU	SELU	SELU	SELU	ELU	SELU	ELU	LEAKY RELU

Table 5. The table displays the hyperparameter values for a 5 day prediction and the baseline models considered.

HYPERPARAM.	LSTM	BiLSTM	RNN	BiRNN	GRU	BiGRU	TRANF.	TCN
LEARNING RATE	0.000731	0.000731	0.000168	5.254E-05	0.000165	0.000572	0.000884	8.053E-05
# NEURONS	190	120	140	190	50	180	-	50
# LAYERS	4	6	2	5	4	2	2	-
SEQUENCE LENGTH	100	100	100	100	100	100	100	100
BATCH SIZE	160	160	160	160	160	160	80	120
DROPOUT RATE	0.29	0.37	0.32	0.23	0.36	0.23	0.27	0.41
ACTIVATION FUNCTION	SELU	ELU	SELU	SELU	PRELU	PRELU	LEAKY RELU	SELU

Table 6. The table displays the hyperparameter values for a 20 day prediction and the baseline models considered.

HYPERPARAM.	LSTM	BiLSTM	RNN	BiRNN	GRU	BiGRU	TRANF.	TCN
LEARNING RATE	0.000899	5.518E-05	0.000818	8.943E-05	0.000371	0.000117	0.000206	0.000178
# NEURONS	180	60	70	20	180	140	-	30
# LAYERS	6	5	3	10	6	8	2	-
SEQUENCE LENGTH	100	100	100	100	100	100	100	100
BATCH SIZE	80	160	80	160	160	80	160	160
DROPOUT RATE	0.25	0.49	0.28	0.22	0.42	0.19	0.30	0.36
ACTIVATION FUNCTION	SELU	ELU	ELU	RELU	SELU	ELU	LEAKY RELU	ELU

C.2. Time-Geometric Model

The Time-Geometric model comprises three components, as elucidated in Section 4. For the Time Component, we adopt the same hyperparameters as those for the baseline models, as delineated in Tables 4, 5, and 6, respectively, for predictions of 1, 5, and 20 days. Concerning the Geometric Component, the hyperparameters encompass the dropout rate, the number of neurons and layers for the Graph Convolutional Network, the number of neurons for the LSTM layer, the presence of the dropout rate, and the specification of whether an undirected graph, denoted as “None”, or a directed graph, denoted as “L-TO-R” (Left-to-Right), is considered to represent the time series. Conversely, the hyperparameters in the Fully Connected Component involve the consideration of the skip layer and the activation function, which, for simplicity, is set to match the activation function found in the baseline model. Tables 7, 8, and 9 outline the hyperparameters for the Time-Geometric model corresponding to prediction horizons of 1, 5, and 20 days.

Table 7. The table displays the hyperparameter values for a 1 day prediction and the Time-Geometric model, denoted as TG, with the Time Component model values enclosed in brackets.

HYPERPARAM.	TG(LSTM)	TG(BiLSTM)	TG(RNN)	TG(BiRNN)	TG(GRU)	TG(BiGRU)	TG(TRANF.)	TG(TCN)
DROPOUT RATE	0.37	0.02	0.22	0.48	0.33	0.05	0.37	0.24
# NEURONS	40	190	110	90	160	120	110	60
# LAYER	9	9	7	7	8	10	2	7
# NEURONS LSTM	40	20	100	30	180	30	180	80
DROPOUT?	TRUE	FALSE	TRUE	TRUE	TRUE	FALSE	TRUE	TRUE
SKIP LAYER	TRUE	TRUE	FALSE	TRUE	TRUE	TRUE	TRUE	TRUE
DIRECTION	L-TO-R	NONE	L-TO-R	NONE	L-TO-R	L-TO-R	NONE	NONE

Table 8. The table displays the hyperparameter values for a 5 day prediction and the Time-Geometric model, denoted as TG, with the Time Component model values enclosed in brackets.

HYPERPARAM.	TG(LSTM)	TG(BiLSTM)	TG(RNN)	TG(BiRNN)	TG(GRU)	TG(BiGRU)	TG(TRANF.)	TG(TCN)
DROPOUT RATE	0.25	0.17	0.13	0.4	0.06	0.03	0.03	0.01
# NEURONS	140	80	160	180	30	100	150	160
# LAYER	5	7	10	2	6	7	5	10
# NEURONS LSTM	160	170	20	130	190	100	130	80
DROPOUT?	FALSE	TRUE	TRUE	TRUE	TRUE	TRUE	TRUE	TRUE
SKIP LAYER	TRUE	TRUE	TRUE	FALSE	TRUE	TRUE	TRUE	TRUE
DIRECTION	L-TO-R	NONE	L-TO-R	NONE	NONE	L-TO-R	NONE	NONE

Table 9. The table displays the hyperparameter values for a 20 day prediction and the Time-Geometric model, denoted as TG, with the Time Component model values enclosed in brackets.

HYPERPARAM.	TG(LSTM)	TG(BiLSTM)	TG(RNN)	TG(BiRNN)	TG(GRU)	TG(BiGRU)	TG(TRANF.)	TG(TCN)
DROPOUT RATE	0.21	0.15	0.11	0.13	0.05	0.45	0.08	0.29
# NEURONS	130	160	110	160	190	20	90	180
# LAYER	5	2	6	5	9	2	2	3
# NEURONS LSTM	50	20	190	170	80	20	190	50
DROPOUT?	FALSE	FALSE	TRUE	FALSE	TRUE	FALSE	TRUE	FALSE
SKIP LAYER	FALSE	TRUE	FALSE	TRUE	FALSE	FALSE	FALSE	FALSE
DIRECTION	NONE	NONE	NONE	NONE	L-TO-R	NONE	NONE	L-TO-R

D. Results

In this section, we present the results of the evaluation metrics for all the models considered in the analysis.

D.1. Evaluation Metrics Results

Tables 10 and 11 present the results for all the models under consideration for the evaluation metrics, namely Root Mean Square Error (RMSE), Mean Absolute Error (MAE), Mean Absolute Percentage Error (MAPE), and Mean Absolute Scaled Error (MASE), for the 5 and 20 day prediction, respectively. It is important to note that a smaller value indicates better performance relative to the others. The best-performing model for each metric is highlighted in bold.

Table 10. The table displays the average metric values for a 5 day prediction across all models in the considered dataset. In parentheses, we specify the Time Component considered in the Time-Geometric model, denoted in the table as TG. The best-performing model for each metric is highlighted in bold.

MODEL	RMSE	MAE	MAPE	MASE
LSTM	4.0979	3.0234	1.9594	1.3064
BiLSTM	5.7802	4.2239	3.1294	2.0567
RNN	3.1201	2.3216	1.5447	1.0180
BiLSTM	3.0803	2.2928	1.5426	1.0238
GRU	2.6417	2.0466	1.2799	0.8665
BiGRU	3.0593	2.3167	1.4362	0.9515
TRANSF.	9.4793	7.1196	4.8149	3.1075
TCN	8.3543	6.2987	4.3513	2.8774
TG(LSTM)	2.5442	1.7810	1.2149	0.7979
TG(BiLSTM)	4.4332	2.8562	2.1135	1.3274
TG(RNN)	2.6913	1.8169	1.2785	0.8272
TG(BiLSTM)	3.1389	2.3015	1.5676	1.0375
TG(GRU)	2.1209	1.6391	1.0352	0.6921
TG(BiGRU)	2.7205	2.0417	1.2581	0.8224
TG(TRANSF.)	2.3148	1.7685	1.1219	0.7554
TG(TCN)	3.5292	2.5441	1.8232	1.1920

Table 11. The table displays the average metric values for a 20 day prediction across all models in the considered dataset. In parentheses, we specify the Time Component considered in the Time-Geometric model, denoted in the table as TG. The best-performing model for each metric is highlighted in bold.

MODEL	RMSE	MAE	MAPE	MASE
LSTM	11.3770	9.0394	6.1697	4.0384
BiLSTM	7.2682	5.7614	3.9615	2.5693
RNN	7.7205	6.1167	3.9599	2.6271
BiLSTM	9.5645	7.4786	5.1974	3.3012
GRU	7.6971	6.1448	4.0830	2.7182
BiGRU	8.2659	6.5398	4.2292	2.8106
TRANSF.	11.0544	8.7913	6.1235	3.9174
TCN	11.8729	8.9351	5.9946	3.8302
TG(LSTM)	12.5783	10.0061	6.7539	4.2900
TG(BiLSTM)	5.6507	4.3606	2.9326	1.9024
TG(RNN)	8.1585	6.5460	4.3116	2.8110
TG(BiLSTM)	9.1312	6.9099	4.9102	3.0900
TG(GRU)	8.8487	7.1136	4.6734	3.0290
TG(BiGRU)	8.4649	6.6535	4.3596	2.9185
TG(TRANSF.)	10.7575	8.5082	5.8595	3.7253
TG(TCN)	12.6266	9.5592	6.2406	3.9679

In Figures 7 and 8, we present histogram plots illustrating the distribution of evaluation metrics for all the models considered, focusing on the forecasting horizons of 5 days and 20 days, respectively.

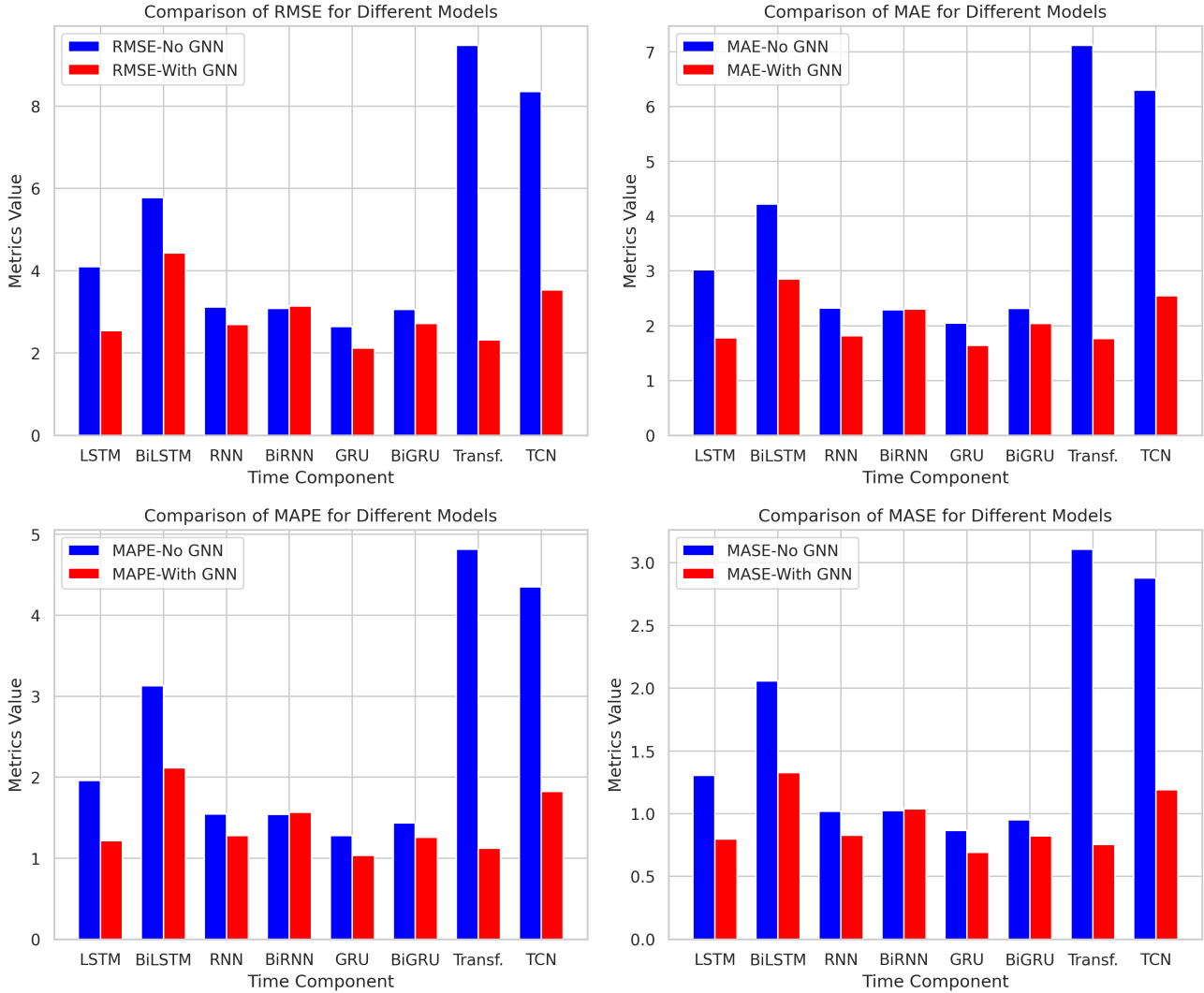


Figure 7. Average metric values for 5 day prediction for all the models within the considered dataset are presented in the figure. The x-axis denotes the models used both as baselines and in the Time Component. The blue bar represents the average metric values for the respective baseline model, while the red bar signifies the average metric value for the Time-Geometric model.

E. Statistical Significance

In this section, we present the statistical significance analysis for all the models considered across various evaluation metrics. We start by detailing the outcomes of pairwise comparisons, followed by an exploration of multiple comparisons.

E.1. Pairwise Comparison

Tables 12 and 13 display the results of the statistical tests conducted to assess potential statistical differences between the baseline models and their implementations including the Time-Geometric model for the 5 and 20 days prediction results, respectively.

E.2. Multiple Comparison

Table 14 presents the average ranks for all the models across different evaluation metrics for the prediction horizons considered in the analysis — specifically, 1, 5, and 20 days. The ranks are computed by comparing the evaluation metrics of

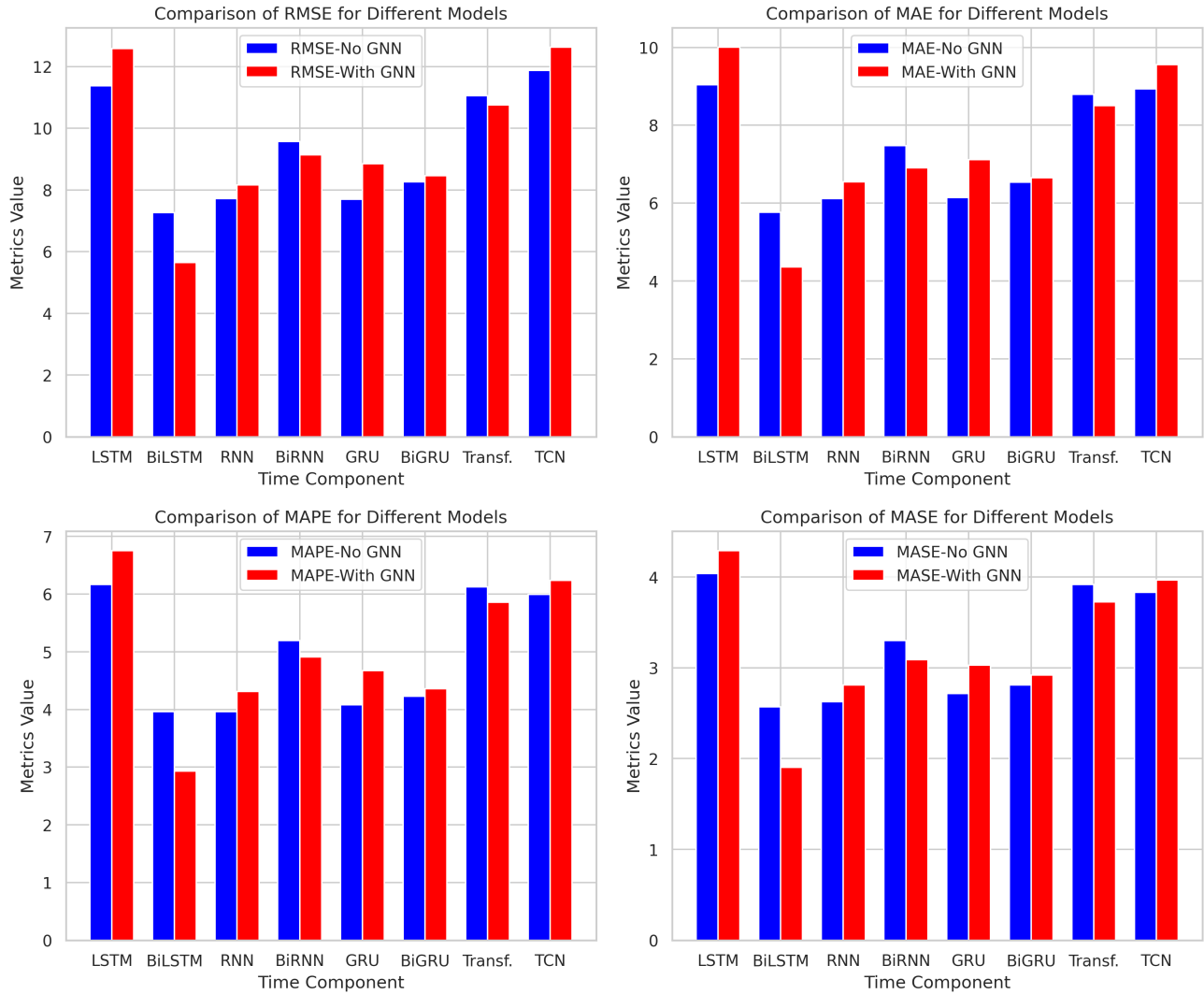


Figure 8. Average metric values for 20 day prediction for all the models within the considered dataset are presented in the figure. The x-axis denotes the models used both as baselines and in the Time Component. The blue bar represents the average metric values for the respective baseline model, while the red bar signifies the average metric value for the Time-Geometric model.

all models for each dataset, assigning the value of 1 to the best results, 2 for the second-best, and so on. The average rank for each model is then computed. It is important to note that a lower rank suggests that the algorithm generally achieved better results compared to other models. Values in bold indicate the best rank for each metric.

In Figures 9 and 10, the results of the Nemenyi test for all the evaluation metrics are presented for the 5 and 20 days forecasting horizons, respectively. This test assesses whether there is a statistically significant difference among the models utilized in the analysis. In the figures, yellow blocks indicate non-statistically significant differences between the models.

The Statistical Significance of the Inclusion of Graph Neural Networks in the Financial Time Series Forecasting Problem

Table 12. The table presents the outcomes of the tests, with Acceptance denoted as *A* and Rejection as *R*. The test statistics for the Paired t-test, Wilcoxon test, and Sign test are encapsulated in brackets. The entry Δ -“*Model*” signifies the comparison between the baseline model and its corresponding Time-Geometric model. For the Paired t-test, we consider 89 degrees of freedom, resulting in a critical value of 1.986. In the Wilcoxon test, the critical value is 1.9599, and for the Sign test, the critical value is 54.42.

MODEL	PAIRED T-TEST				WILCOXON TEST				SIGN TEST			
	RMSE	MAE	MAPE	MASE	RMSE	MAE	MAPE	MASE	RMSE	MAE	MAPE	MASE
Δ LSTM	R(6.0)	R(6.6)	R(9.4)	R(11)	R(8.0)	R(8.1)	R(8.1)	R(8.0)	R(87)	R(88)	R(88)	R(88)
Δ BiLSTM	R(4.4)	R(5.6)	R(6.5)	R(6.4)	R(7.6)	R(7.9)	R(8.1)	R(8.1)	R(84)	R(86)	R(86)	R(86)
Δ RNN	R(4.4)	R(5.6)	R(9.6)	R(8.1)	R(5.9)	R(7.3)	R(7.4)	R(7.1)	R(73)	R(80)	R(80)	R(80)
Δ BiRNN	A(1.2)	A(0.2)	A(0.8)	A(1.1)	R(2.6)	A(0.6)	A(1.0)	A(1.2)	A(30)	A(44)	A(44)	A(43)
Δ GRU	R(4.4)	R(4.4)	R(8.6)	R(5.9)	R(6.7)	R(6.4)	R(6.6)	R(6.4)	R(76)	R(76)	R(76)	R(75)
Δ BiGRU	R(2.1)	R(2.2)	R(2.1)	A(1.9)	R(3.8)	R(3.6)	R(3.6)	R(3.5)	R(60)	R(58)	R(58)	R(57)
Δ TRANSF.	R(7.1)	R(8.0)	R(18)	R(12)	R(8.2)	R(8.2)	R(8.2)	R(8.2)	R(90)	R(90)	R(90)	R(90)
Δ TCN	R(6.1)	R(7.2)	R(16)	R(11)	R(8.2)	R(8.2)	R(8.2)	R(8.2)	R(90)	R(90)	R(90)	R(90)

Table 13. The table presents the outcomes of the tests, with Acceptance denoted as *A* and Rejection as *R*. The test statistics for the Paired t-test, Wilcoxon test, and Sign test are encapsulated in brackets. The entry Δ -“*Model*” signifies the comparison between the baseline model and its corresponding Time-Geometric model. For the Paired t-test, we consider 89 degrees of freedom, resulting in a critical value of 1.986. In the Wilcoxon test, the critical value is 1.9599, and for the Sign test, the critical value is 54.42.

MODEL	PAIRED T-TEST				WILCOXON TEST				SIGN TEST			
	RMSE	MAE	MAPE	MASE	RMSE	MAE	MAPE	MASE	RMSE	MAE	MAPE	MASE
Δ LSTM	A(1.4)	A(1.5)	A(1.5)	A(1.7)	A(1.0)	A(1.0)	A(0.9)	A(1.0)	A(42)	A(41)	A(41)	A(40)
Δ BiLSTM	R(8.7)	R(8.8)	R(9.1)	R(7.5)	R(8.2)	R(8.2)	R(8.2)	R(8.2)	R(89)	R(90)	R(90)	R(89)
Δ RNN	A(1.1)	A(1.5)	A(1.98)	R(2.1)	A(1.7)	R(2.1)	R(2.5)	R(2.5)	A(39)	A(39)	A(39)	A(39)
Δ BiRNN	R(4.9)	R(5.7)	R(8.0)	R(8.3)	R(7.2)	R(7.3)	R(7.1)	R(7.2)	R(81)	R(82)	R(82)	R(80)
Δ GRU	R(2.4)	R(2.5)	R(3.3)	R(3.1)	R(2.5)	R(2.5)	R(2.7)	R(2.6)	A(37)	A(35)	A(35)	A(34)
Δ BiGRU	A(0.5)	A(0.4)	A(1.0)	A(0.9)	A(1.2)	A(0.8)	A(0.8)	A(0.7)	A(40)	A(43)	A(43)	A(39)
Δ TRANSF.	A(1.1)	A(1.2)	R(3.1)	R(2.5)	R(4.0)	R(3.9)	R(3.8)	R(3.8)	R(66)	R(66)	R(66)	R(66)
Δ TCN	A(1.1)	A(1.2)	A(1.2)	A(1.0)	A(1.5)	R(2.1)	A(1.8)	A(1.8)	A(40)	A(34)	A(34)	A(33)

Table 14. The table presents the average ranks for the algorithms computed on each dataset. Values in bold indicate the best rank for each metric.

MODEL	1-DAY				5-DAY				20-DAY			
	RMSE	MAE	MAPE	MASE	RMSE	MAE	MAPE	MASE	RMSE	MAE	MAPE	MASE
LSTM	5.71	6.86	6.78	6.86	10.92	11.23	11.05	11.23	12.38	12.40	12.41	12.40
BiLSTM	7.50	8.12	8.17	8.12	13.95	13.94	13.96	13.94	5.10	5.10	5.20	5.10
RNN	8.21	8.78	8.67	8.78	8.52	8.50	8.48	8.50	5.54	5.66	5.55	5.66
BiRNN	4.86	6.46	6.24	6.46	8.63	8.93	8.93	8.93	10.02	10.05	10.15	10.05
GRU	13.74	13.90	13.90	13.90	5.51	6.22	6.05	6.22	5.87	5.93	5.86	5.93
BiGRU	6.05	5.90	5.92	5.90	5.13	5.55	5.52	5.55	6.70	6.82	6.67	6.82
TRANSF.	15.75	15.65	15.67	15.65	15.27	15.34	15.30	15.34	12.47	12.61	12.68	12.61
TCN	14.07	14.92	14.81	14.92	15.18	15.25	15.27	15.25	11.27	10.65	10.54	10.65
TG(LSTM)	5.34	4.57	4.56	4.57	4.90	4.43	4.44	4.43	12.90	13.11	13.08	13.11
TG(BiLSTM)	6.91	5.07	5.24	5.07	12.11	11.21	11.42	11.21	1.50	1.35	1.38	1.35
TG(RNN)	8.07	8.34	8.37	8.34	6.23	5.05	5.20	5.05	6.42	6.64	6.62	6.64
TG(BiRNN)	4.74	5.28	5.32	5.28	9.15	8.77	8.86	8.77	8.36	7.94	8.22	7.94
TG(GRU)	13.60	12.46	12.57	12.46	2.18	2.51	2.44	2.51	7.27	7.43	7.40	7.43
TG(BiGRU)	7.60	5.15	5.28	5.15	3.96	4.26	4.30	4.26	7.21	7.33	7.34	7.33
TG(TRANSF.)	12.56	12.48	12.52	12.48	3.47	3.85	3.78	3.85	11.63	11.70	11.74	11.70
TG(TCN)	1.23	1.97	1.90	1.97	10.82	10.90	10.93	10.90	11.30	11.23	11.08	11.23

Nemenyi Test for Evaluation Metrics with 5 day forecasting horizon

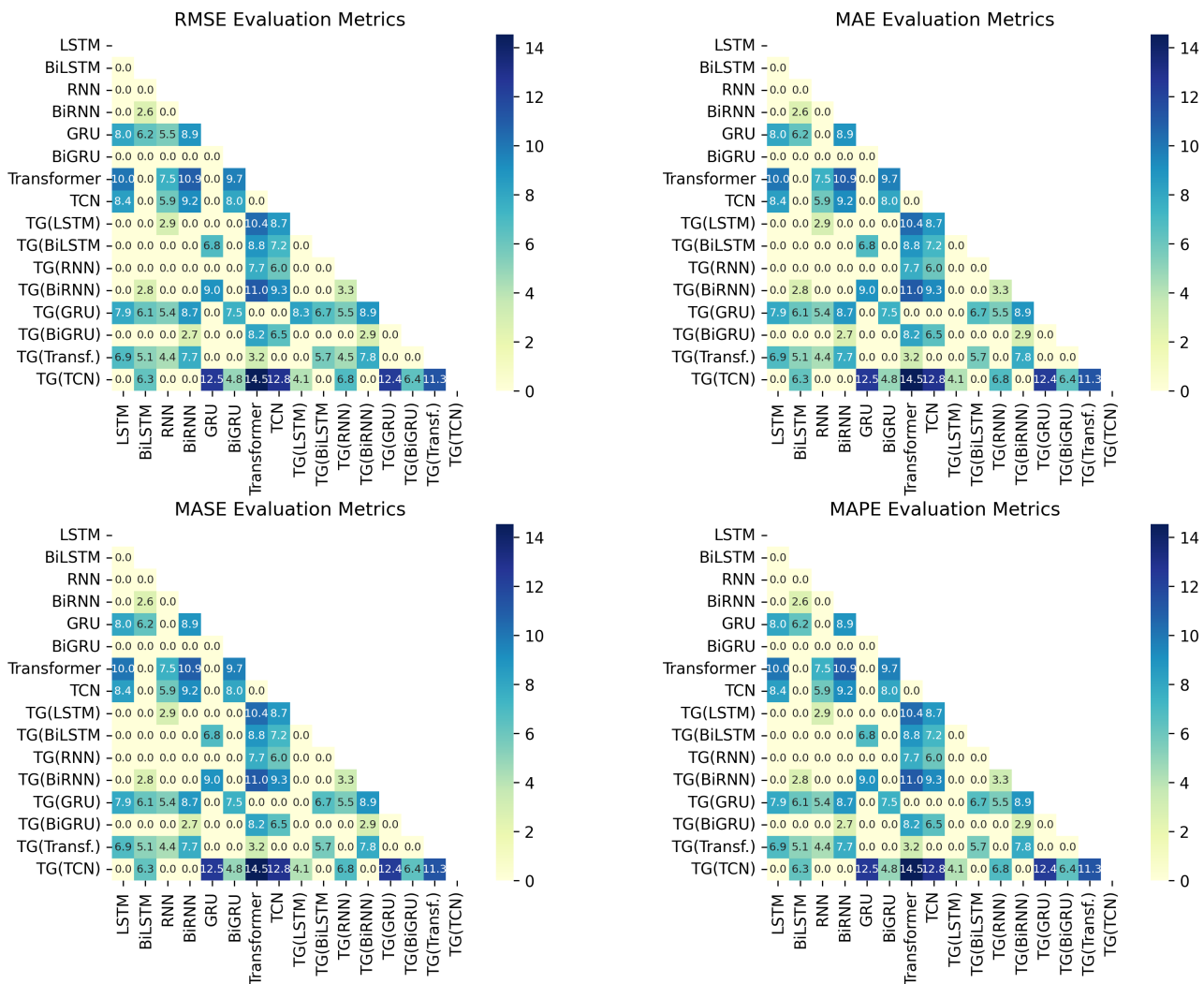


Figure 9. Nemenyi test for 5 day forecasting. Non-statistically significant relationship are highlighted in yellow.

Nemenyi Test for Evaluation Metrics with 20 day forecasting horizon

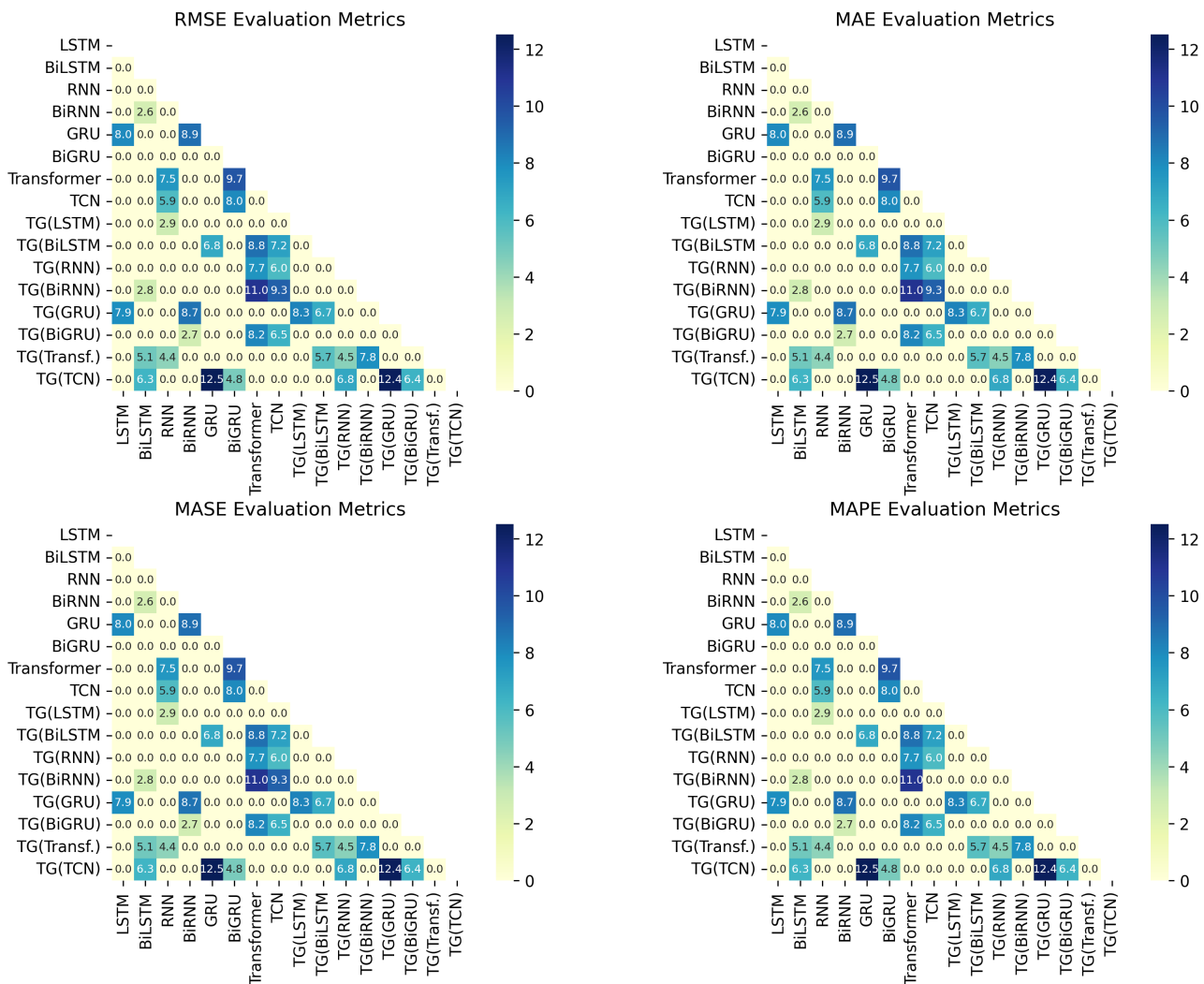


Figure 10. Nemenyi test for 20 day forecasting. Non-statistically significant relationship are highlighted in yellow.